Analytical High-efficiency Spot-beam Model for High Throughput Satellites

Peter BALLING

ASC Antenna Systems Consulting ApS, Selsmosevej 12, 2630 Taastrup, Denmark

pballing@asc-consult.dk

Abstract. *We develop a simple model for a feed horn with a uniformly excited circular aperture at the focus of an offset paraboloidal reflector antenna and compare it with reflector antenna analyses using combinations of circular waveguide TE_{1n} modes. The model demonstrates the deep dip that can occur at the spot-beam center for certain feed diameters and it is used in a design procedure that relates the feed and the spot-beam diameter. The model may be extended to include feed horn flare effects.*

Keywords

Satellite antenna, multibeam antenna, offset reflector, circular waveguide feed, high-efficiency feed, high throughput satellite.

1. Introduction

Single-feed-per-beam multiple spot-beam reflector antenna systems, where the feeds are divided among three or four offset paraboloidal reflector apertures to achieve both a high crossover level and a low spillover loss, have become very popular for Ka-band high throughput satellites [1], [2], [3]. Recent European examples include Avanti Hylas-2 launched Aug. 2012 and EUTELSAT Ka-Sat launched Dec. 2010. The latter provides a throughput of more than 70 Gb/s from about 80 spot beams distributed over four 2.6m reflectors [4]. The throughput may increase to the Tb/s range on future satellites with more, smaller beams from larger reflectors operating over wider and also higher frequency bands [5].

Initially these interleaved spot-beam reflectors had feeds with essentially a Gaussian pattern so that well-established design rules apply. Later so-called high-efficiency horns with ideally uniform aperture illumination have attracted much attention as a means to provide higher performance or more degrees of freedom in the design. Here we use the term high-efficiency horn to indicate any horn that aims at a realizing a uniform aperture distribution. Circular hard horns are one candidate, e.g. implemented by longitudinal corrugations achieving low crosspolarization (< -30 dB) and high aperture efficiency

(> 88%) over 10-15% bandwidth [6]**.** It is difficult to extend this high-efficiency mode to wide or dual bands such as combined Rx/Tx operation. The comprehensive review of hard (and soft) horns in [7] indicates that some progress in low-index ($\varepsilon_r < 1$) metamaterials is desirable in order to achieve low crosspolarization for the very wide bandwidth (> 100%) that may be obtained by soft horns with axial or radial corrugations.

So far circular multi-mode horns with combinations of TE_{1n} modes to approximate a uniform horn aperture field have been preferred as no dielectrics are required and no aperture area is lost to corrugations or additional layers. In [8] a 5λ-diameter horn with three steps to excite the higher-order modes gave 10% bandwidth for a crosspolarization of -30 dB, an aperture efficiency of 86% and a return loss of 25 dB. A larger horn diameter requires more TE_{1n} higher-order modes. Degrading effects include that the modal spectrum at the horn aperture in practice deviates from the optimum one, only propagating TE_{1n} modes may be included, and in particular the feed aperture efficiency is degraded by the phase variation across the horn aperture. The crosspolarization level may be a good measure of the deviation of the mode spectrum from the ideal one. Several patents have been claimed in the area of multi-mode high-efficiency feeds and impressive performance can be obtained as indicated in the following despite the many modes considered.

The issues of Tx and Rx beam equalization and of non-uniform lattices with differently sized spot beams have been addressed in [9] for a Ka-band Tx/Rx antenna system with four 1.9m reflectors. For beam equalization, one approach is to optimize the feed horn to equalize the Tx and Rx reflector far fields benefiting from feed sidelobes that at Rx fall on the reflector and flatten and widen the Rx secondary beam. An irregular lattice with both 0.7° and 1.08° beams was realized by increasing the feed size for the wider beams. At Rx this comes at a price as a noticeable dip develops at the center of the wide beam – see Fig. 20 in [9]. This point is discussed further below. The reported feed horn performance over the Tx bands 18.3-18.8 and 19.7-20.2 GHz and the Rx bands 28.35-28.6 and 29.25 to 30.0 GHz (both about 10%) is aperture efficiency about 80%, crosspolarization more than 25 dB below peak, and return loss better than 25 dB.

Details of another Ka-band dual-band dual-polarized high-efficiency feed horn are given in [10], [11]. This design uses four slope discontinuities to excite up to TE$_{13}$ in the Tx band and up to TE$_{15}$ in the Rx band. The horn diameter is about 58 mm and the length about 118 mm. The measured worst-case performance over three frequencies in the Tx band (18.3-20.2 GHz) / three frequencies in the Rx band (28.3-30 GHz) are 83.8 / 83.1% for aperture efficiency, −18.8 / −23.1 dB for crosspolarization, and 24.2/ 27.6 dB for return loss indicating a different feed efficiency and crosspolarization trade-off than in [9]. The horn pattern plots (Fig. 4 in [11]) show the relatively high crosspolarization at 18.3 GHz and that about half the first sidelobe at 30 GHz falls inside the reflector rim at about 18°.

In the following we derive an analytic model for the far field from an offset paraboloidal reflector illuminated by an ideal high-efficiency feed horn with a uniform aperture distribution. Next we consider some special cases, provide a validation of the simple model, and set up a procedure to determine the feed diameter that will provide a desired spot-beam beamwidth or vice versa. This model is particularly useful in the initial design to determine the relation between the feed horn diameter and the reflector spot-beam beamwidth when an antenna system with a complex non-uniform spot-beam lattice shall be designed. We use a standard root-finding procedure with a closed-form expression that provides the effects of the reflector parameters on the beamwidth given the feed diameter. Otherwise several physical-optics reflector analyses would be required. The complete multi-feed multi-reflector antenna analyses with accurately measured or calculated feed pattern data required for the full design and performance evaluation are not dealt with here. However, we investigate the problem that may occur when a deep dip develops at the spot-beam center for certain feed diameters. If a satellite user is located near these dips, it may be necessary to allocate more resources in terms of power and bandwidth as is done for users near the edge of coverage. Finally the extension of the model to include feed horn flare effects and the use of the feed horn flare to control the beam-center dips are briefly discussed.

2. Derivation of the Spot Beam Model

The feed far-field pattern (normalized to isotropic level, but neglecting the Huygens' factor as justified by the large feed sizes and small angles subtended by the reflectors normally used, horn flare etc.) from a uniformly illuminated circular aperture of diameter d is

$$f(\theta,\phi) = \frac{2J_1\left(\frac{\pi d}{\lambda}\sin\theta\right)}{\sin\theta} \qquad (1)$$

corresponding to an ideal high-efficiency feed with 100% aperture efficiency. In (1), which is derived in numerous texts, the diameter d is normalized with the wavelength λ

and $J_n(x)$ is the Bessel function of the first kind and order n (here $n = 1$). The reflector-antenna far field from this ideal feed at the reflector focus may be determined within the Physical Optics approximation by Jacobsen's "reflector transformation" [12] of the feed pattern integrated over the reflector surface, i.e.

$$E_P(\Theta,\Phi,R) = \frac{-j}{\lambda}\frac{e^{-jkR}}{R}\int_0^{\theta^*}\int_0^{2\pi}\frac{2J_1\left(\frac{\pi d}{\lambda}\sin\xi\right)}{\xi} \times \qquad (2)$$
$$e^{jk(xU+yV+zW-r)}\,r\sin\xi\,d\psi\,d\xi$$

where θ^* is the half angle subtended by the reflector rim as seen from the focus, (U, V, W) the reflector far-field direction cosines, (x, y, z) the reflector surface coordinates, and r the distance from the feed to the reflector surface point.

By means of the following approximations valid for a feed at the focus of the offset paraboloid with focal length f and offset angle θ_o:

$$xU+yV+zW-r \approx 2f\frac{\xi\sin\Theta\cos(\psi-\Phi)}{1+\cos\theta_o}, \qquad (3)$$

$$r\sin\xi \approx \frac{2f}{1+\cos\theta_o}\xi, \qquad (4)$$

$$\sin\xi \approx \xi, \qquad (5)$$

the reflector transformation (2) simplifies to

$$E_P(\Theta,\Phi,R) \approx -j\frac{e^{-jkR}}{R}\frac{4kf}{1+\cos\theta_o} \times$$
$$\int_0^{\theta^*}J_1\left(\frac{\pi d}{\lambda}\xi\right)J_0\left(\frac{2kf\sin\Theta}{1+\cos\theta_o}\xi\right)d\xi \qquad (6)$$

With these approximations the spot-beam pattern from the offset reflector becomes rotational symmetric.

It has not been possible to express the finite integral

$$I_{\theta^*} = \int_0^{\theta^*}J_1(\alpha\xi)J_0(\beta\xi)d\xi \qquad (7)$$

where

$$\alpha = \frac{\pi d}{\lambda} \qquad (8)$$

$$\beta = \frac{2kf\sin\Theta}{1+\cos\theta_o} \qquad (9)$$

in closed form in the general case. The integral (7) may be evaluated as a Gaussian hypergeometric series [13]. As our implementation of this approach suffered from numerical instability for large values of α and β - in the order of 200 or more where the integrand becomes highly oscillatory, we chose to integrate the finite integral (7) numerically either using the algorithm "*quad*" available in Python

Scipy and Matlab or directly in Maple. Typical values of α and β for a 100λ reflector are up to 10-30. In following we consider some special cases.

2.1 Infinitely Large Reflector

An infinitely large reflector may be simulated if θ^* approaches infinity. Then, the corresponding infinite integral (7) may be expressed in closed form [14]

$$I_\infty(\alpha,\beta) = \frac{1+\text{sign}(\alpha-\beta)}{2\alpha}. \qquad (10)$$

Thus, an infinitely large perfect reflector would generate a uniform circular spot beam with the level $8f/d(1+\cos\theta_o)$, no sidelobes and width $d(1+\cos\theta_o)/2f$ (corresponding to a gain × area product of 4π):

$$\lim_{\theta^*\to\infty} E_P(\Theta,\Phi,R) \approx -j\frac{e^{-jkR}}{R}\frac{4f}{d(1+\cos\theta_o)} \times$$
$$\left(1+\text{sign}\left(\frac{d(1+\cos\theta_o)}{4f}-\sin\Theta\right)\right) \qquad (11)$$

For practical antenna sizes, the performance is limited by diffraction effects that generate gain ripple in the coverage area and sidelobes outside as discussed below.

2.2 Field near the Beam Center

Near the axis Θ and β are close to 0, and the integral (7) simplifies to

$$I_{\theta^*}(\alpha,\beta) \approx \int_0^{\theta^*} J_1(\alpha\xi)\left(1-\frac{(\beta\xi)^2}{4}\right)d\xi$$
$$\approx \frac{1}{\alpha}\left[1-J_0(\alpha\theta^*)-\frac{(\beta\theta^*)^2}{4}J_2(\alpha\theta^*)\right] \qquad (12)$$

which has an oscillatory behavior on the axis versus the feed diameter normalized with the wavelength d/λ around the "infinite" antenna result (11) or "average" level $1/\alpha$. In the region near the beam axis, the field is an interference pattern between a contribution from the central part of the reflector and a smaller contribution due to the axial caustic from the reflector rim.

2.3 Field for "Large" Values of Θ (or β)

We may express (7) as

$$I_{\theta^*}(\alpha,\beta) = I_\infty(\alpha,\beta) - \int_{\theta^*}^{\infty} J_1(\alpha\xi)J_0(\beta\xi)d\xi. \qquad (13)$$

If α, β and θ^* are sufficiently large, we may approximate the Bessel functions in the second term of (13) by their asymptotic expressions

$$J_n(x) \approx \sqrt{\frac{2}{\pi x}}\cos\left(x-\frac{n\pi}{2}-\frac{\pi}{4}\right). \qquad (14)$$

Then, Maple may express the second term in closed form in terms of the sine and cosine integrals Si(x) and Ci(x), and we obtain

$$I_{\theta^*}(\alpha,\beta) \approx \frac{1}{2\alpha}+\frac{\text{sign}(\alpha-\beta)}{2\alpha}\left(1-\sqrt{\frac{\alpha}{\beta}}\right) -$$
$$\frac{\text{Si}((\beta-\alpha)\theta^*)+\text{Ci}((\beta+\alpha)\theta^*)}{\pi\sqrt{\alpha\beta}}. \qquad (15)$$

Obviously this will fail when $\alpha\theta^*$ and $\beta\theta^*$ are less than about 2 and 1, respectively. We will see in Sec. 3 that the combination of the simple approximations (12) near the beam center and (15) near the edge of coverage (EOC) and in the sidelobe region is adequate for practical antennas.

2.4 "EOC" Field at $\alpha = \beta$

At the "edge-of-coverage" angle we have from (7)

$$I_{\theta^*}(\alpha,\alpha) = \int_0^{\theta^*} J_1(\alpha\xi)J_0(\alpha\xi)d\xi$$
$$= \frac{1}{2\alpha}\left[1-J_0^2(\alpha\theta^*)\right] \qquad (16)$$

which is less than (or equal to) half the average or asymptotic coverage-area level $1/\alpha$ (11). This level is too low to be useful as the spot-beam crossover level and an alternative crossover determination will be developed in Sec. 3.

2.5 Spillover Efficiency

As the ideal feed pattern (1) is normalized to isotropic level, our analyses include a spillover loss. The spillover efficiency is defined by the fraction of the power radiated by the feed that is intercepted by the reflector. If (5) applies, the spillover efficiency is

$$\eta_{SO} = 1-J_0^2(\alpha\theta^*)-J_1^2(\alpha\theta^*). \qquad (17)$$

3. Numerical Results and Discussion

Fig. 1 compares the reflector transformation model (6) in dashed blue line with a more rigorous analysis by the general reflector antenna software package Grasp in red lines for a circularly polarized 1.5m offset paraboloidal reflector antenna at 20.2 GHz for a 60mm feed (left) and a 80mm feed (right). For the offset reflector $f/D = 1.6$, the offset angle $\theta_o = 44.41°$ and the subtended half angle $\theta^* = 15.21°$.

The uniformly illuminated circular waveguide feed is modeled in Grasp by the first three TE_{1n} modes assuming
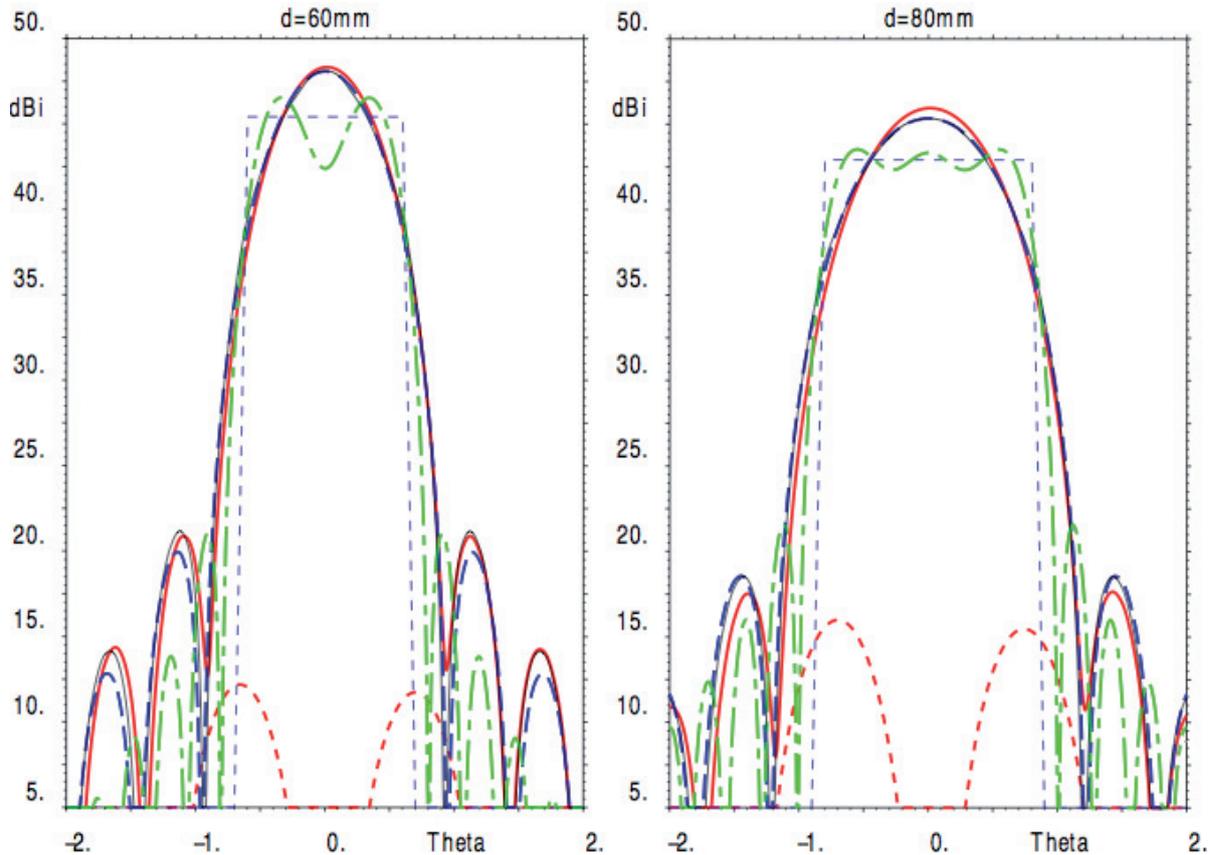
Fig. 1. Tx co- and crosspolar field at 20.2 GHz calculated by Grasp for 1.5m RHCP offset reflector (full and dotted red curves), by transformation model (6) (dashed blue curve), by infinite antenna model (11) (thin dotted blue curve), by transformation model for 3m reflector (dash-dot green curve), and by closed-form model (12) and (15) (thin black curve) for 60mm feed (left) and 80mm feed (right). Note the dip at center of the beam for the 3m reflector for the smaller feed.

ideal modal amplitude ratios 1:0.295:0.182. The agreement between the copolar fields (full red line and dashed blue line) is good – in particular for the smaller feed where three TE_{1n} modes more accurately model the uniform aperture illumination. The crosspolar field in dotted red line predicted by Grasp and the different on-axis directivity levels indicate the deviation of the feed from an ideal one. In practice it is not possible to approximate this closely the ideal mode distribution and the crosspolarization will be significantly higher as we have seen above. Also a small circular polarization beam squint (about 0.02°) appears on the plots.

The figure also shows the "infinite" antenna result (11) in thin blue dotted line and the transformation model result for a 3m reflector in dash-dot green line. The "infinite" antenna or "average" field level is equal to 45.4 dBi for $|\Theta| < 0.61°$ and zero outside for the smaller feed, and equal to 42.9 dBi for $|\Theta| < 0.82°$ and zero outside for the larger feed. While the beam shapes are essentially that of a pencil beam for the 1.5m reflector, the beam shapes become more "flat topped" for the 3m reflector with three large ripples for the 60mm feed and five smaller ripples for the 80mm feed.

Finally the figure shows the "asymptotic" result (15) in thin black line (mostly hidden by the dashed blue curve). This field is singular as $\sin^{-0.5}\Theta$ at $\Theta = 0$ so that the "near-axis" field result (12) is used for $\beta\theta^* < 1$ where the asymptotic expression (14) for $J_o(\beta\xi)$ fails. It is surprising that the combination of (12) and (15) works so well, but we adopt this combination as the "closed-form" result.

It is evident that increasing the reflector size can significantly improve the EOC directivity even though the additional reflector surface is only weakly illuminated by feed-pattern sidelobes. However, there is a potential for deep on-axis minima due to the axial caustic. The larger reflector has more rapidly decaying sidelobes.

For a small reflector the beam shaping capabilities is limited by diffraction or the minimum foot print size - about 0.69° for the 1.5m reflector at 20.2 GHz.

Fig. 2 shows similar patterns plots at 30 GHz. Due to the higher frequency, the uniformly illuminated circular waveguide feed is now modeled by the first four TE_{1n} modes with modal amplitude ratios 1:0.295:0.182:0.133. Now the deep on-axis gain loss occurs even for the 1.5 m reflector for the 80mm feed. For the 3m reflector there are
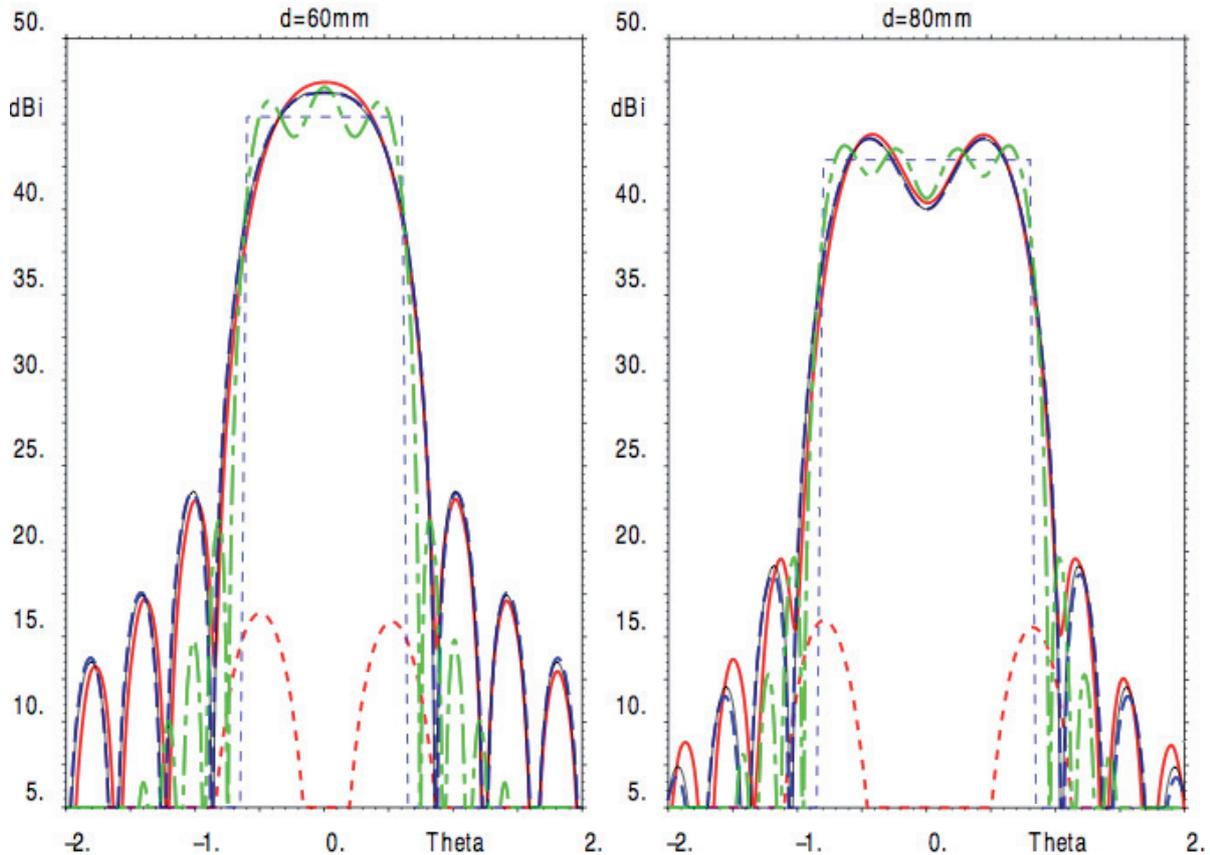
Fig. 2. Rx co- and crosspolar field at 30 GHz calculated by Grasp for 1.5m RHCP offset reflector (full and dotted red curves), by transformation model (6) (dashed blue curve), by infinite antenna model (11) (thin dotted blue curve), by transformation model for 3m reflector (dash-dot green curve), and by closed-form result (12) and (15) (thin black curve) for 60mm uniform feed (left) and 80mm uniform feed (right). Note the dip at center of the beam for both the 1.5m and the 3m reflector for the larger feed.

five gain ripples for the smaller feed and seven gain ripples for the larger feed.

3.1 On-axis Gain Variation

The on-axis gain variation due to the axial caustic can be problematic. The pattern is rotationally symmetric and a very small power can significantly change the on-axis field. It is expected that a modification of the feed or the reflector near the rim may reduce the problem.

Fig. 3 shows the on-axis directivity derived from (12) at 20.2 and 30 GHz and the average coverage-area level derived from (11) versus feed diameter d for the 1.5m reflector. It is seen that the 80mm feed dimension is close to the minimum for the on-axis level at 30 GHz. The parameter $\alpha\theta^*$ in (12) varies between 2.25 and 6.75 at 20.2 GHz and between 3.34 and 10.02 at 30 GHz.

The deepest minimum occurs at $\alpha\theta^* = 7.016$, where the field at the beam center is 3.1 dB below the average level. This case should probably be avoided and the feed diameter remain below or above

$$d_o = 2.233\frac{\lambda}{\theta^*} \tag{18}$$
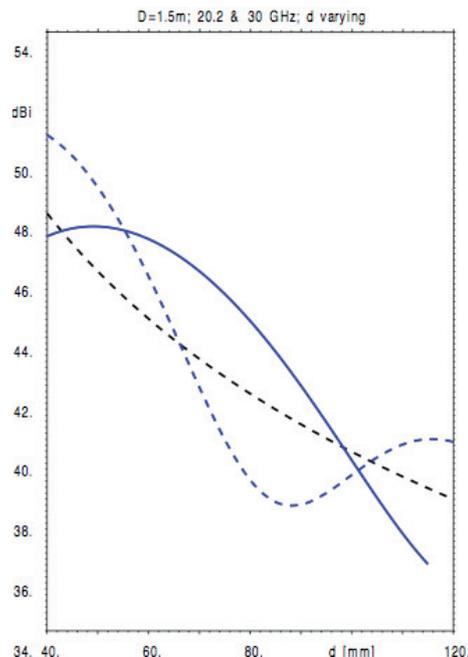
Fig. 3. "Infinite" antenna directivity level (dotted black curve) and on-axis directivity at 20.2 GHz (full blue curve) and 30 GHz (dotted blue curve) versus feed diameter d for 1.5m reflector.

or the satellite operator may be required to allocate more resources to users near the spot-beam center. The next slightly more shallow on-axis minimum occurs for $\alpha\theta^* = 13.324$ and is about 2.1 dB below the average level.

3.2 Beamwidth versus Feed Diameter

The field (16) at the edge-of-coverage angle $\sin\Theta_{EOC} = d(1 + \cos\theta_o)/4f$ for the infinitely large reflector is 6 dB (or slightly more) lower than the average coverage-area level. A more appropriate EOC angle for initial antenna design work is desirable. We have not been able to derive a simple formula for this angle, but propose a procedure where a root is found from the asymptotic expression (15) normalized by the average level $1/\alpha$. Fig. 4 shows this asymptotic pattern and the deviation from the transformation integral (7) versus Θ/Θ_{EOC}. The region near $\Theta = 0$, where the asymptotic pattern is singular, is excluded. The four different values of $\alpha\theta^*$ cover the range 3.37 – 6.67 used in Fig. 1 and 2 and include one value close to 7.016 where the deepest dip at the spot-beam center occurs. Close to Θ_{EOC}, the error in finding the angle that corresponds to a specified level becomes smaller due to the steeper pattern slope.

Based on the asymptotic pattern and Brent's root-finding algorithm [15], a simple and very fast Fortran program is used to find an approximate EOC angle corresponding to a level of 0 to 4 dB below the average level $1/\alpha$, or conversely find the feed diameter d given the beamwidth, by equating (15) to the desired level. In the first instance β (or the beamwidth) is determined given α (or the feed diameter), and in the second instance α given β. Tab. 1 illustrates the accuracy of this approach for the first instance assuming either the asymptotic pattern (15) or the accurate representation (7). The agreement is good and the error will be less than, e.g. those caused by bandwidth effects and practical feeds deviating from the ideal feed model (1).

4. Feed Horn Flare Effects

The model may be extended to include horn flare effects represented by a quadratic phase across the feed aperture, e.g. in terms of Lommel functions of two variables. The present case with a uniform amplitude distribution corresponds closely to that of von Lommel's diffraction problem from 1885 with a circular aperture in a screen illuminated by a spherical wave. The detailed approach for extending the feed pattern (1) is explained in [16] and previously used for horn analysis in [17].

$\alpha\theta^*$	Asymp. pattern	Accurate pattern	Error [%]
3.08	0.7970	0.7855	1.5
4.41	0.7918	0.7928	-0.12
7.06	0.8900	0.8889	0.12
9.72	0.9286	0.9277	0.10

Tab. 1. Relative edge-of-coverage angle $x = \Theta/\Theta_{EOC}$ determined from asymptotic and accurate pattern vs. $\alpha\theta^*$.
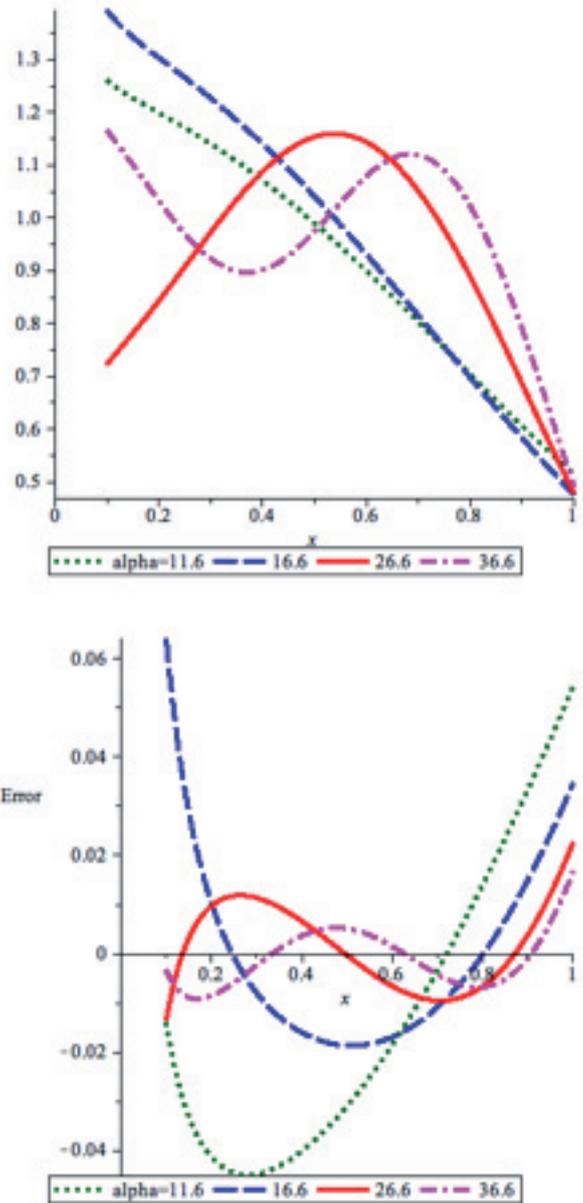
Fig. 4. Normalized patterns for $\alpha\theta^* = 3.08$, 4.41, 7.06 and 9.72 versus relative angle $x = \Theta/\Theta_{EOC}$. Asymptotic pattern (15) (top) and difference between accurate pattern and asymptotic pattern (bottom).

Two expressions are obtained: one inside the feed cone and another outside the feed cone for best convergence of the Bessel function expansions of the Lommel functions. The two expressions have a wide overlap region. The horn flare widens the feed pattern and generates a phase error across the reflector aperture. For the range of parameters considered in Sec. 3, the effect on the reflector far field is small for small half flare angles like 5°. For intermediate half flare angles like 10° and in particular 15°, the effect is significant. While the reflector beamwidth is fairly insensitive to the feed flare angle, the sidelobes increase and the field near the beam center is very sensitive. Thus, the asymptotic pattern (15) can be used to find the beamwidth for small to moderate feed flare angles. Refocusing the feed by moving its phase center to the reflector focus has

unwanted effects. The feed phase pattern is important and it can be shown that with the flared feed aperture located at the focus, a (very) large reflector will eventually recover the ideal shape (11), but with a phase pattern superimposed. Thus, the horn flare may control the spot-beam center dip.

5. Conclusion

After a review of recent circular high-efficiency feed horns, we presented a far-field model for offset paraboloidal reflector antennas with ideal high-efficiency feeds. The model provides insight into the underlying physics, and is useful in initial trade-offs for satellite single-feed-per-beam multiple spot-beam reflector antenna systems to determine the relation between feed and spot-beam diameter given the reflector geometry. The model is also useful in identifying when dips occur at the spot-beam centers degrading the communications capability. The extension to horn flare effects and their impact on the reflector far field have been addressed.

Acknowledgements

References

[1] INGERSON, P., CHEN, C. A. The use of non-focusing aperture for multibeam antenna. In *Proc. IEEE International Symposium on Antennas and Propagation*. Houston (TX), 1983, p. 330-333. [Note: While the title refers to an alternative multiple spot-beam solution based upon an oversized hyperboloidal reflector, the paper also discusses the multiple reflector aperture case].

[2] RAO, S. K. Design and analysis of multiple-beam reflector antennas. *IEEE Antennas and Propagation Magazine*, Aug. 1999, vol. 45, no. 4, p. 53-59.

[3] RAO, S. K. Parametric design and analysis of multiple-beam reflector antennas for satellite communications. *IEEE Antennas and Propagation Magazine*, Aug. 2003, vol. 45, no. 4, p. 26-34.

[4] http://en.wikipedia.org/wiki/KA-SAT.

[5] NELSON, N. J. G., AUGEVAIN, J.-C., MANGENOT, C. Toward the Terabit/s satellite: Antenna trade-offs and analyses. In *Proc. 33rd ESA Antenna Workshop*. Noordwijk, Oct. 2011, paper 14.4.

[6] SOTOUDEH, O., KILDAL, P.-S., INGVARSON, P., SKOBELEV, S. P. Single- and dual-band multimode hard horn antennas with partly corrugated walls. *IEEE Transactions on Antennas and Propagation*, Feb. 2006, vol. 54, no. 2, p. 330-339.

[7] LIER, E. Review of soft and hard horn antennas, including meta-material-based hybrid-mode horns. *IEEE Antennas and Propagation Magazine*, Apr. 2010, vol. 52, no. 2, p. 31-39.

[8] BHATTACHARYYA, A. K., GOYETTE, G. A novel horn radiator with high aperture efficiency and low cross-polarization and applications in arrays and multibeam reflector antennas. *IEEE Transactions on Antennas and Propagation*, Nov. 2004, vol. 52, no. 11, p. 2850-2859.

[9] AMYOTTE, E., DEMERS, Y., MARTINS-CAMELO, L., BRAND, Y., LIANG, A., UHER, J., CARRIER, G., LANGEVIN, J.-P. High performance communications and tracking multi-beam antennas. In *Proc. 1st European Conference on Antennas and Propagation*. Nice (France), Nov. 2006, Paper 359671.

[10] RAO, S. K. TANG, M. Q. Stepped reflector antenna for dual-band multiple beam satellite communications payloads. *IEEE Transactions on Antennas and Propagation*, Mar. 2006, vol. 54, no. 3, p. 801-811.

[11] RAO, S., CHAN, K. K., TANG, M. Design of high efficiency circular horn feeds for multibeam reflector applications. In *IEEE International Symposium on Antennas and Propagation*. Washington, DC, 2005, p. 359-362.

[12] JACOBSEN, J. On the crosspolarization of asymmetric reflector antennas for satellite applications. *IEEE Transactions on Antennas and Propagation*, 1977, vol. 25, p. 276-283.

[13] POCHERNYAEV, V. N. Integrals of products of Bessel functions for applied electrodynamic problem. *Ukrainian Math. Journ.*, 1995, vol. 47, p. 658-662.

[14] GRADSHTEYN, I. S., RYZNIK, I. M. *Table of Integrals, Series, and Products*. New York, NY: Academic Press, 1980. Eq. 6.512 3. p. 667.

[15] http://en.wikipedia.org/wiki/Brent%27s_method.

[16] BORN, M., WOLF, E. *Principles of Optics*. Cambridge, UK: Cambridge University Press, 6th ed., 1980, Sec. 8.8.1.

[17] NARASIMHAN, M. S., RAO, B. V. Radiation from conical horns with large flare angles. *IEEE Transactions on Antennas and Propagation*, Sep. 1971, vol. 19, p. 678-681.

About Authors ...

Peter BALLING received his MScEE and PhD from the Technical University of Denmark in 1969 and 1972, respectively. He was 1972-1974 with the Department. of Electrical Engineering, University of Zambia, teaching telecom courses. In the periods 1974-1981 and 1984-1989 he was with TICRA, a consulting company in Copenhagen. From 1981 to 1984 he was with the R & D department at INTELSAT, Washington, D.C., involved in satellite multi-beam antennas. Since 1989 he is an independent consultant in ASC, Antenna Systems Consulting. Specific capabilities include satellite multibeam and contoured-beam antennas, reflector and feeds systems, and microwave beamforming networks. Since 1985 he has participated in seven antenna COST Actions and served as secretary to several. For more information, see http://www.asc-consult.dk.